Electronic Supplementary Material (ESI) for Lab on a Chip.


# Enhanced ion transport using geometrically structured charge selective interfaces: Supplementary Information

Anne M. Benneker,[†] Burcu Gumuscu,[‡,¶] Ernest G.H. Derckx,[†] Rob G.H. Lammertink,[†] Jan C.T. Eijkel,[‡] and Jeffery A. Wood[*,†]

†*Soft Matter, Fluidics and Interfaces, MESA+ Institute for Nanotechnology, University of Twente, The Netherlands*

‡*BIOS Lab-on-a-Chip Group, MESA+ Institute for Nanotechnology, MIRA Institute for Biomedical Technology and Technical Medicine, University of Twente, The Netherlands*

¶*Current address: Department of Bioengineering University of California, Berkeley California, USA*

E-mail: j.a.wood@utwente.nl

## S1. FLIM calibration

For the quantification of the $Cl^-$ concentration in the microchannels by Fluorescence-Lifetime Imaging Microscopy (FLIM), a calibration curve for is constructed. A modified Stern-Volmer equation[1] (Equation 1, where $\tau$ is the measured lifetime, $c$ is the concentration and $A$,$f$ and $K$ are fitting parameters) can be used to fit the concentration over the measured concentration range from 0.01 to 10 mM.

$$\tau = A(1 - \frac{1}{\frac{1}{fKc} + \frac{1}{f}}) \quad (1)$$

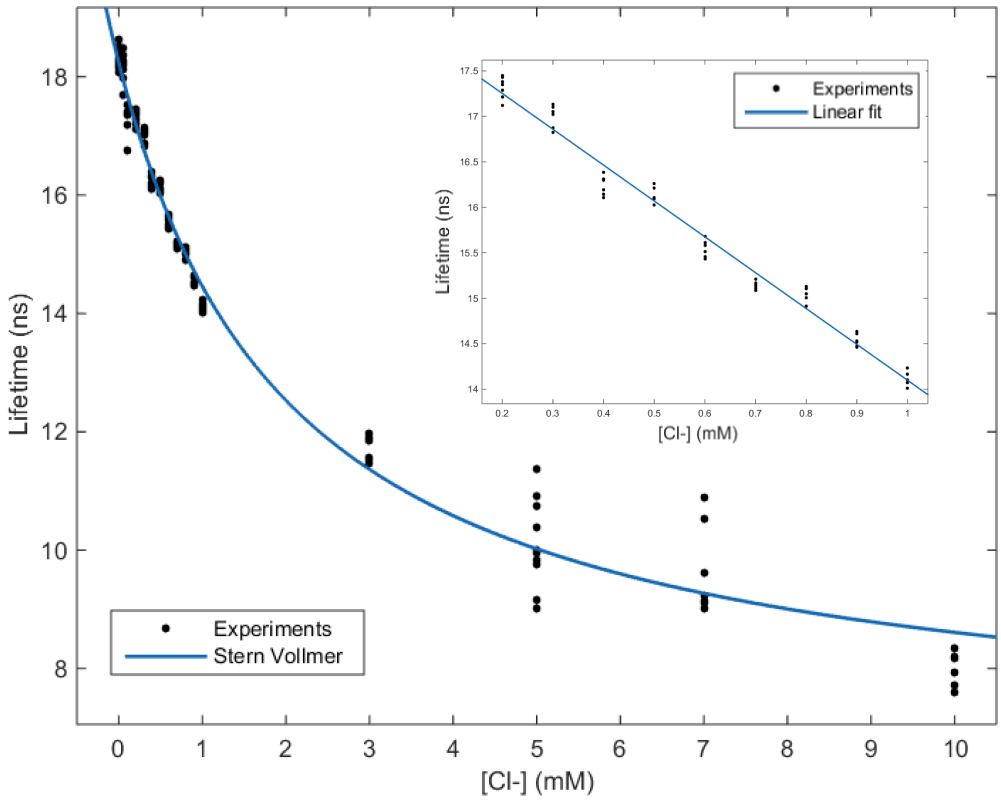


Figure 1

This fit is shown in Figure S1, where one can observe that especially for higher concentrations the spread in measurements is large. Therefore, we are only measuring in the linear regime between 0.2 and 1 mM (shown in the inset of Figure S1), resulting in a higher accuracy in our measurements, also based on the resulting normal probability plots of both fits. For the linear fit ($\tau = a * c + b$) we found the $a = -3.942 \pm 0.154$ and $b = 18.04 \pm 0.1$.

## S2. Current and current density

The measured absolute current for the different geometries at different flow rates is shown in Figure S2. For a more fair comparison between the different geometries, the current density is a better measure.

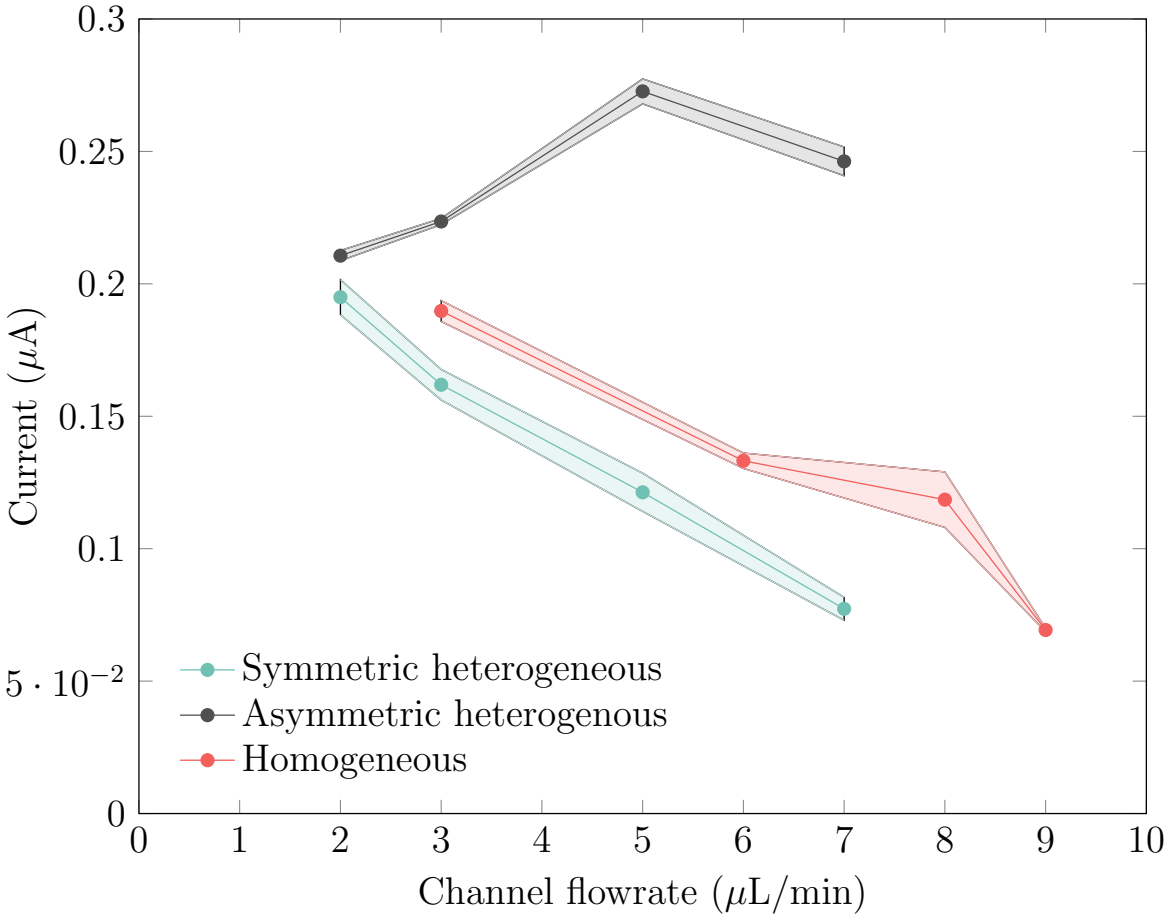


Figure 2

For calculation of the current density (Figure 2b in the manuscript) from the absolute current, the hydrogel area for all different geometries is required. This is calculated using the width ($w_1$ and $w_2$) and height ($h$) of the hydrogels in the channels and the number of patches ($n$), per Equation 2. The values of the different dimension are shown in Table 1.

$$S = n * h * \frac{w_1 + w_2}{2} \tag{2}$$

Table 1: Hydrogel dimensions

| Configuration | $n$ | $h(\mu\text{m})$ | $w_1(\mu\text{m})$ | $w_2(\mu\text{m})$ |
|---|---|---|---|---|
| Trapezoidal heterogeneous | 5 | 67.5 | 295 | 1725 |
| Rectangular heterogeneous | 5 | 67.5 | 690 | 690 |
| Homogeneous | 1 | 67.5 | 16100 | 16100 |

# S3. EOF simulation

To illustrate the role of EOF in driving ion-transport in the heterogeneous system, we make use of a simple simulation framework based on imposing an EOF slip-velocity coupled to the electric-field distribution in our system. Various combinations of zeta-potentials for the hydrogels (positively and negatively charged) and PDMS walls (negatively charged) were considered. In all cases, a recirculation flow can be observed which would aid in ion-transport towards the hydrogel interfaces. In Figure S3, an example of this is provided for the symmetric heterogeneous hydrogels. A single patch is modeled with symmetry along the hydrogel half-plane.

For the COMSOL simulation, the electric field profile is determined by solving the Laplace equation with imposed potential boundary conditions and the velocity profile is determined by solving the Navier-Stokes equations with an imposed wall EOF (Smoluchowski, as in the main text of the paper). The velocities shown in Figure S3 are obtained using zeta-potentials of -100 mV for the negative walls and cation exchange hydrogel and 100 mV for the anion exchange hydrogel The applied electric potential was 0.5 V.

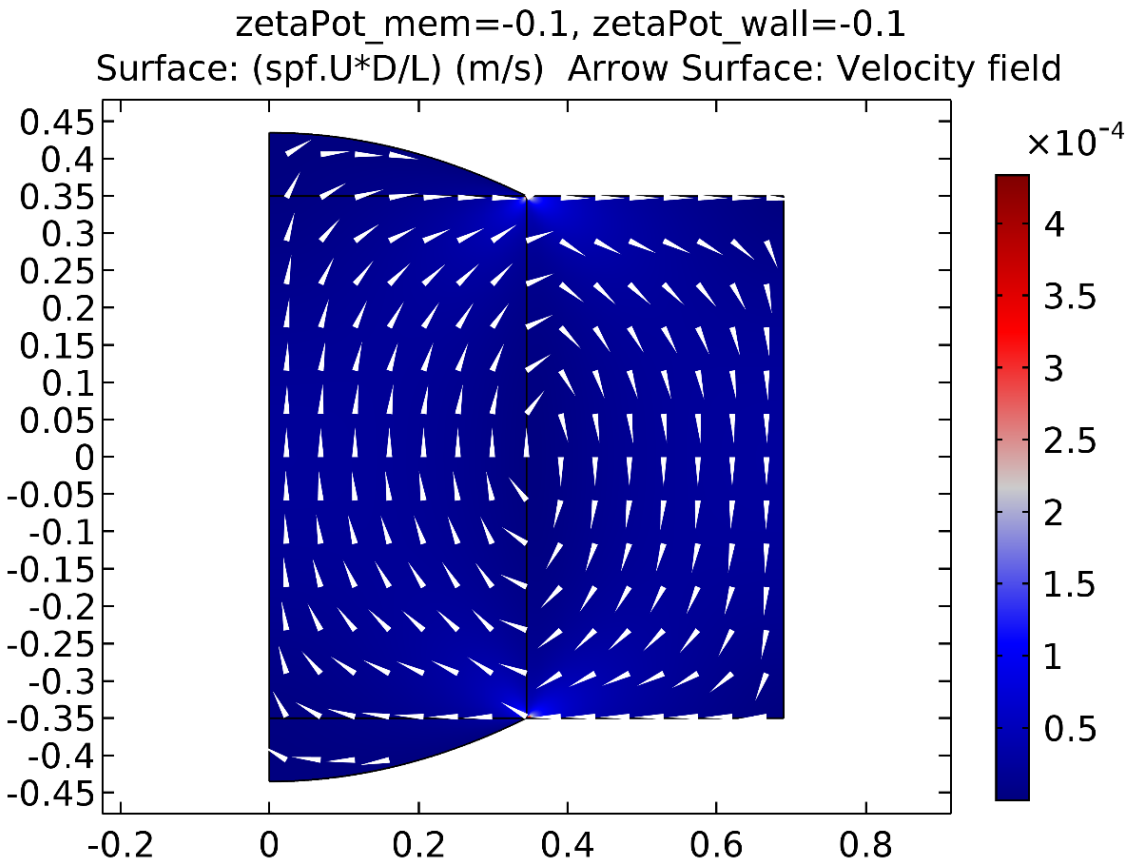


Figure 3: Modeled EOF in the heterogeneous hydrogel geometry.

## S4. Movie 1: Ion depletion zones at homogeneous hydrogel

Development of ion depletion zones at a homogeneous hydrogel under the application of a constant potential of 9V. The configuration is corresponding to the configuration of Figure 3a in the manuscript. The movie is sped up ten times. At first instance, a depletion zone spanning the entire hydrogel is formed, that breaks down in small circular depletion zones at the hydrogel interface. Depletion zones are moving parallel to the interface as a result of EOF and other forces induced by the electric field and the space charge. At elevated times, a concentrated slug is formed in the microchannel, which is surrounded by large ion depletion zones. This movie shows a large similarity to numerical predictions of the ion concentration

at a homogeneous membranes as reported earlier,[2] and shown in their supplementary video S4.

## S5. Movie 2: Ion depletion zones at rectangular heterogeneous hydrogels

Ion depletion at a rectangular heterogeneous hydrogel, in the configuration shown in Figure 3b with a constant applied voltage of 9V. Ion depletion zones form at the hydrogel interface in the lower channel while zones of increased intensity are formed at the discontinuity between the hydrogel and the PDMS pillar. Multiple small depletion zones merge into large depletion zones at the hydrogel. As a function of time, the zones of increased intensity are reduced, only leaving one on the most left hydrogel (the outermost hydrogel on that side).

## S6. Movie 3: Ion depletion zones at trapezoidal heterogeneous hydrogels

Development of ion depletion zones at asymmetric, trapezoidal heterogeneous hydrogels, in the configuration as depicted in Figure 3c. The applied voltage is 9V. In the lower channel, above the smaller hydrogel interface, a single ion depletion zone is forming, while at the larger hydrogel interface multiple small ion depletion zones are forming that merge to larger depletion zones as a function of time. At the hydrogel/PDMS interface, ion concentration is locally increased. Vortical movement of the more concentrated plugs can be observed, yielding mixing of the fluid at these locations.

## S7. FLIM results

In our FLIM measurements, we obtain a quantification of local $Cl^-$ concentration as function of time for all locations where there is a fluorescence signal. Especially in the enriched channel this is valuable as here the enrichment of ions can be monitored. In the depleted channel, the fluorescent dye is depleted as well as it has a negative charge. Therefore, results shown here are only the enriched channels.

By averaging the lifetime along the mid-line of the enriched channel for all times, we can see the development of the ion concentration in time. These developments can be compared for the different geometries. However, the standard deviation between the different measurements and the variance in concentration in the channel yields a large uncertainty in the measured values of concentration. We can plot the average concentration in the upper channel as a function of time for all different configurations of hydrogel and applied current or potential.

An example of such a measurement is shown in Figure S4, where the FLIM results of chronopotentiometric measurements in heterogeneous, rectangular hydrogel chips are shown. In this figure, the error bars are not shown for ease of reading the figure. Especially at lower times, the error bars are largely overlapping. What can be observed is that as a function of time the concentration in the concentrated channel is increasing, as is expected. It seems that this is happening faster for higher applied currents, which would also be according to expectations, but no firm conclusions can be drawn from this based on the confidence intervals of the measurements.

The only conclusion that can be drawn based on the FLIM measurements is that the $Cl^-$ concentration in the enriched channel is increasing as a function of time, for all geometries and all applied currents and voltages. No quantification of the transport rate of ions can be done based on these measurements, since the confidence intervals are too large to draw unambiguous conclusions.

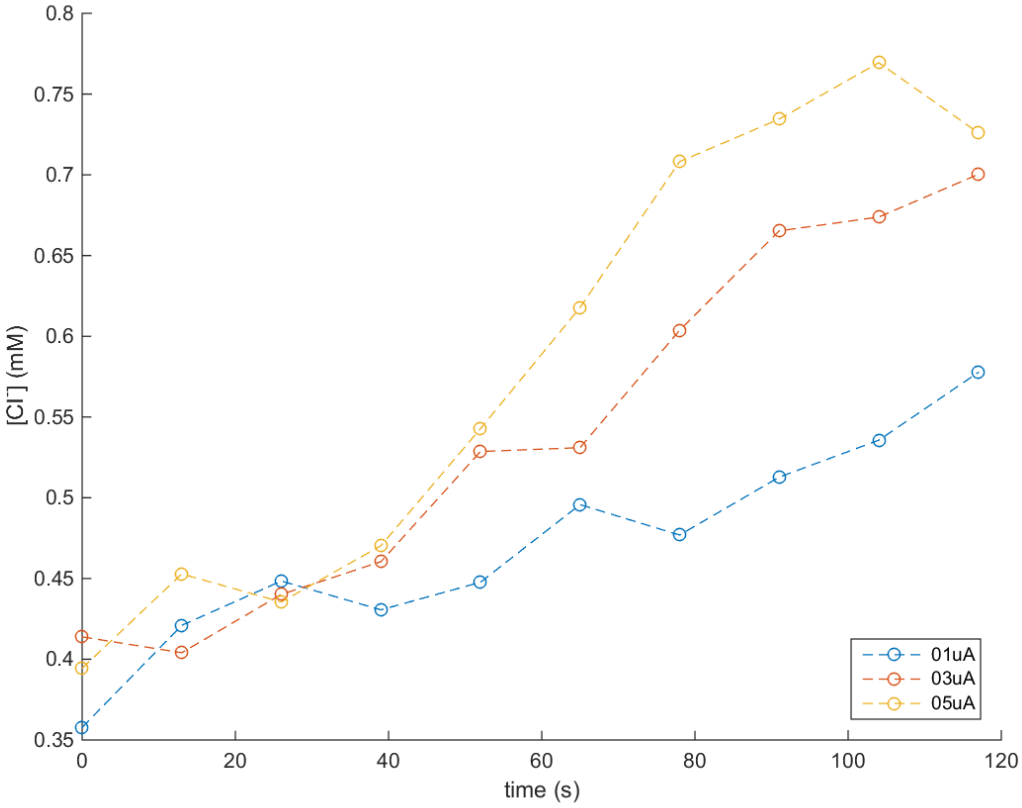


Figure 4

# References

(1) Lakowicz, J. *Principles of Fluorescence Spectroscopy*, 3rd ed.; Springer, New York, 2013.

(2) Davidson, S. M.; Wessling, M.; Mani, A. *Sci. Rep.* **2016**, *6*, 22505.